Electronic Supplementary Information (ESI)†

NaCl-templated synthesis of soybean-derived nitrogen-rich mesoporous carbon material: Iron phthalocyanine integration for four-electron oxygen reduction†

Vikram Rathour[1], Smita Singh[1], Varsha Singh[1], Devesh Kumar Singh[2], Vaibhav Verma[1,3], Piyush Kumar Sonkar[4], and Vellaichamy Ganesan[1,*]

1: Department of Chemistry, Institute of Science, Banaras Hindu University, Varanasi-221005, Uttar Pradesh, India

2: Kutir Post Graduate College, Chakkey, Jaunpur-222146, Uttar Pradesh, India

3: Naval Materials Research Laboratory, Ambernath-421506, Maharashtra, India,

4: Department of Chemistry, MMV, Banaras Hindu University, Varanasi, 221005, Uttar Pradesh, India

* Corresponding author

E-mail: *velganesh@yahoo.com* and *velgan@bhu.ac.in*

† Electronic Supplementary Information is available: Figures and Tables as mentioned in the text.

Preparation of samples for post-catalysis analyses

Indium tin oxide (ITO) coated glass plates were cut into 1 × 3 cm dimensions and a 50 µL of FePc@SN950 suspension was coated on 1 × 1 cm and dried at room temperature. ORR catalysis was performed by carefully dipping only the coated surface area of the ITO glass plate in an oxygen-saturated electrolyte. For post-catalysis analyses (powder XRD and Raman), the electrodes after being subjected to the ORR catalysis for two hours (amperometry at -0.5 V (SCE) in oxygen-saturated conditions) were taken out from the electrolyte, rinsed well with triple distilled water, and dried at room temperature and used. For SEM mapping and EDAX, the ITO plates were carefully cut into small pieces and used.

Table S1 Percentage of nitrogen species in the SN850, SN950, and SN1050 materials

Material	Graphitic N %	Pyrrolic N %	Pyridinic N %	Oxided N %
SN850	**27.69**	**36.23**	**27.03**	**6.82**
SN950	**29.90**	**40.22**	**27.04**	**9.36**
SN1050	**35.15**	**36.02**	**15.88**	**12.99**

Table S2 The Tafel slope values of different materials

Sample	Tafel slope ($mVdec^{-1}$)	
	Basic	**Acidic**
S850	**187**	**381**
S950	**177**	**317**
SN850	**110**	**220**
SN950	**107**	**200**
SN1050	**115**	**215**
FePc@SN950	**91**	**146**
Pt/C	**87**	**88**

Table. S3 The charge transfer resistance (R_{ct}) and solution resistance (R_s) of different materials

Material	Rs (ohm)	R_{ct} (ohm)
S850	65.51	164.4
S950	56.61	38.57
SN850	54.19	16.08
SN950	40.66	10.32
SN1050	49.2	12.16
FePc@SN950	43.7	10.16

Table S4. Comparison of the ORR efficiency of FePc@SN950 with other catalysts in basic medium in terms of E_{onset} and $E_{1/2}$ values

Biomass	**Materials**	**Synthesis strategy**	**E_{onset} (RHE)**	**$E_{1/2}$ (RHE)**	**References**
Willow catkin	Co_3O_4/NCMTs[A]	Pyrolysis in Ar, Pyrolysis with Co precursor in Ar, NH_3	0.906 V	0.778 V	S1
Corn silk	N-P-Fe-C[B]	Hydrothermal, freeze drying, pyrolysis in NH_3, pyrolysis with $FeCl_3$ in NH_3 atmosphere	0.95 V	0.85 V	S2
Rice husk	FeTPP/RHC[C]	Pre-carbonized in Ar, washing with NaOH, activated with HNO_3, pyrolysis with FeTPP	0.95 V	0.88	S3
Water hyacinth root	WHR700[D]	Pyrolysis with $ZnCl_2$, Acid treatment	0.94 V	0.78 V	S4
Soya milk	Fe-N/C-700[E]	Soya milk freeze dry with $FeCl_3$, carbonization, acid washing	0.91 V	0.82 V	S5
Soya bean	FePc@SN950	Carbonization with NaCl, acid wash, immobilization FePc with the help of stirring	0.97	0.89	This work
Peanut shell	CoOP@bio-C[F]	Carbonized with $Co(OH)_2$ and NaH_2PO_2 in N_2, activated with help of CO_2	0.91 V	0.81 V	S6

[A] Cobalt oxide nanoparticle-modified N-doped hollow hierarchical porous carbon microtubes, [B] Nitrogen, phosphorous, and iron tri-doped nanoporous carbon catalyst, [C] Iron tetraphenyl porphyrin calcined with rice husk carbon, [D] Water hyancinth root pyrolyzed at 700 ºC, [E] Iron-nitrogen co-doped carbon, [F] Cobalt oxide phosphite nanoparticles doped biomass carbon

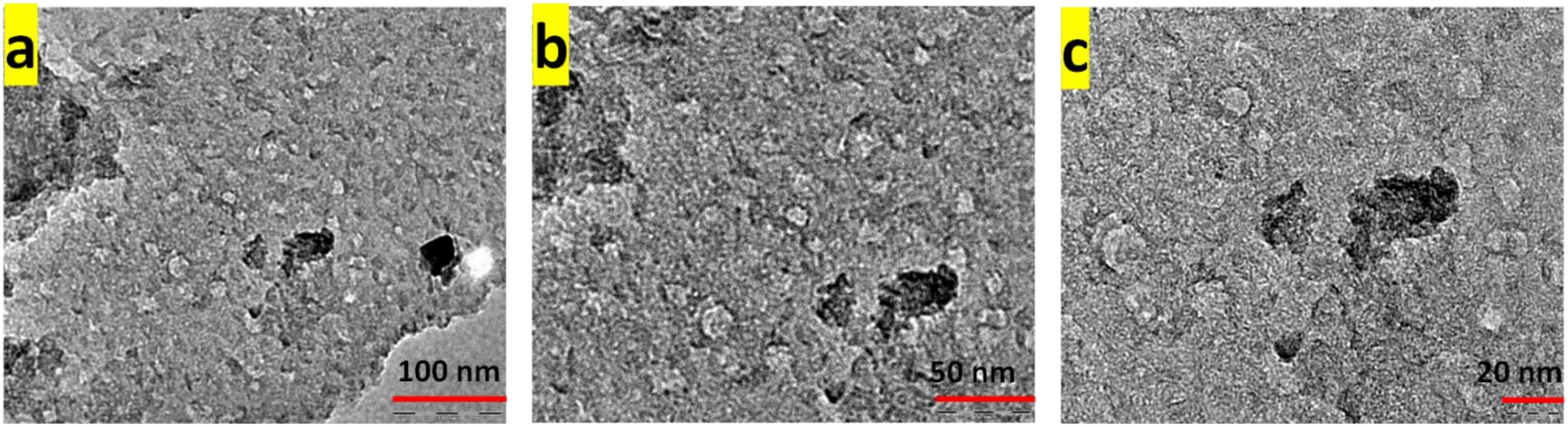

Fig. S1 TEM images of FePc@SN950 at different magnifications (scales: 100 nm (A), 50 nm (B), and 20 nm (C)).

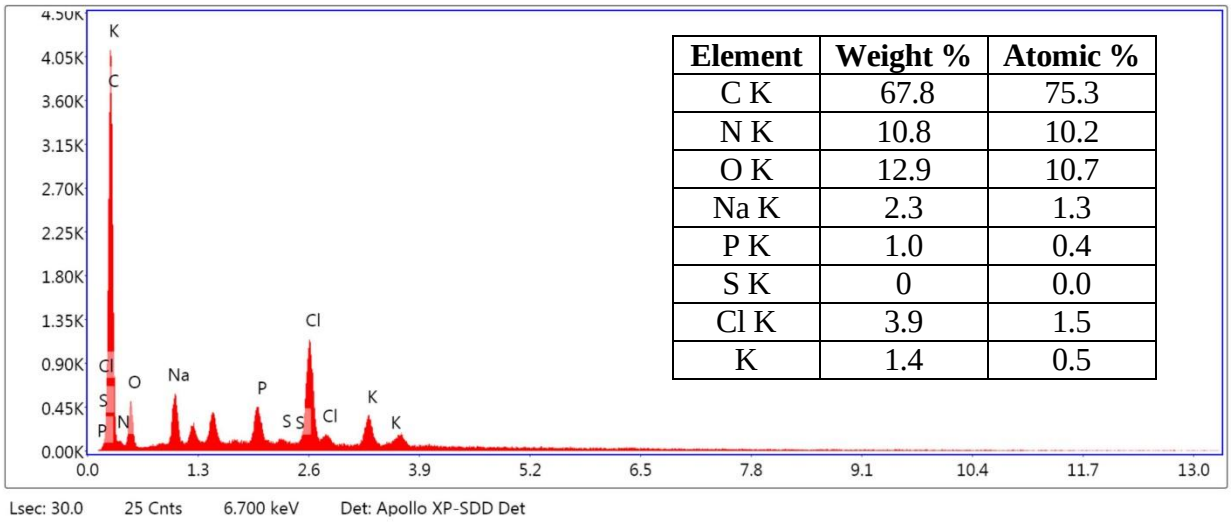

Element	Weight %	Atomic %
C K	67.8	75.3
N K	10.8	10.2
O K	12.9	10.7
Na K	2.3	1.3
P K	1.0	0.4
S K	0	0.0
Cl K	3.9	1.5
K	1.4	0.5

Fig. S2 EDAX spectrum of SN950 showing the presence of expected elements. The inset shows the corresponding elemental composition data.

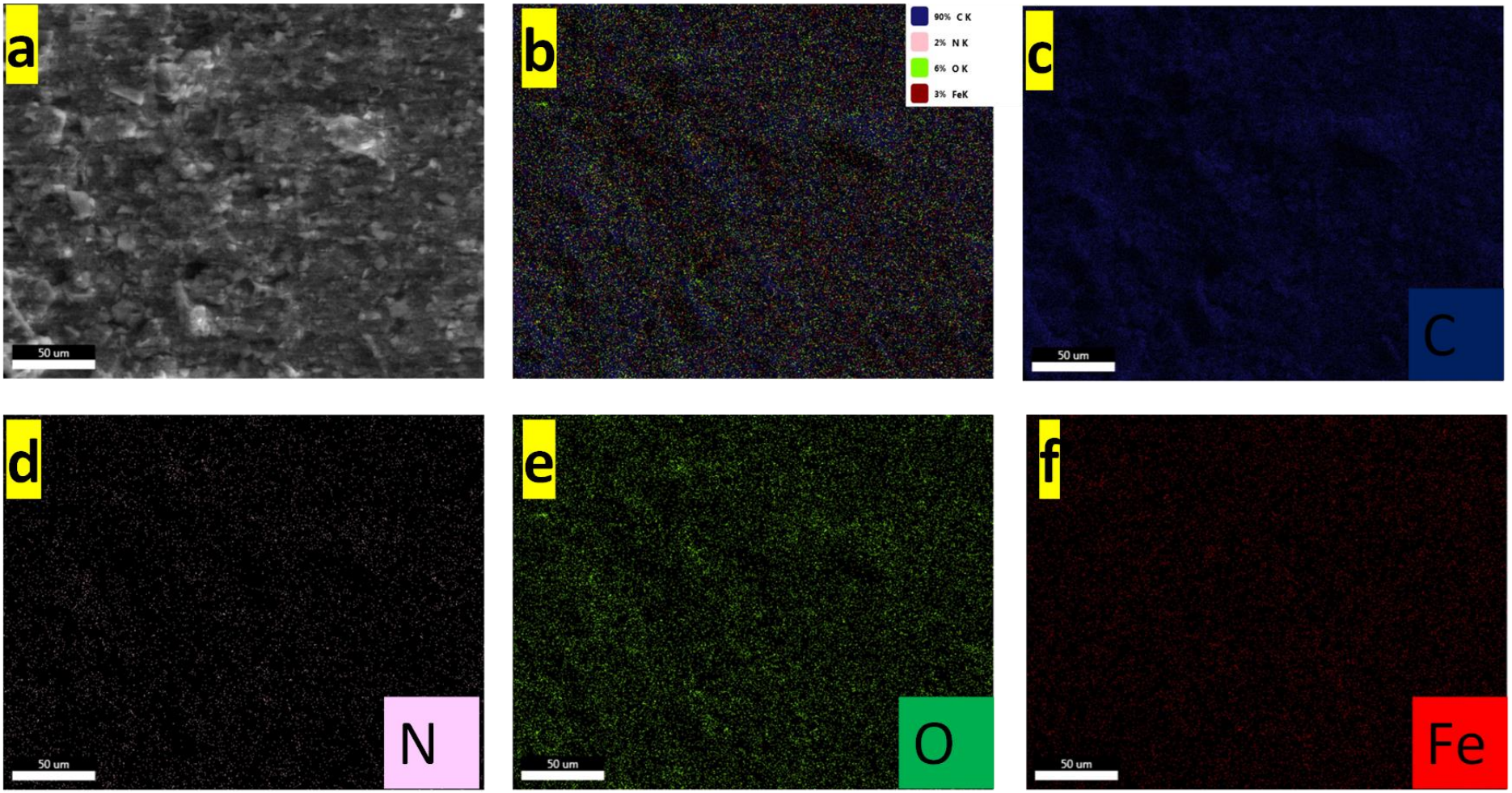

Fig. S3 Pre-catalysis SEM mapping images (a-f) of FePc@SN950 on ITO coated glass plates.

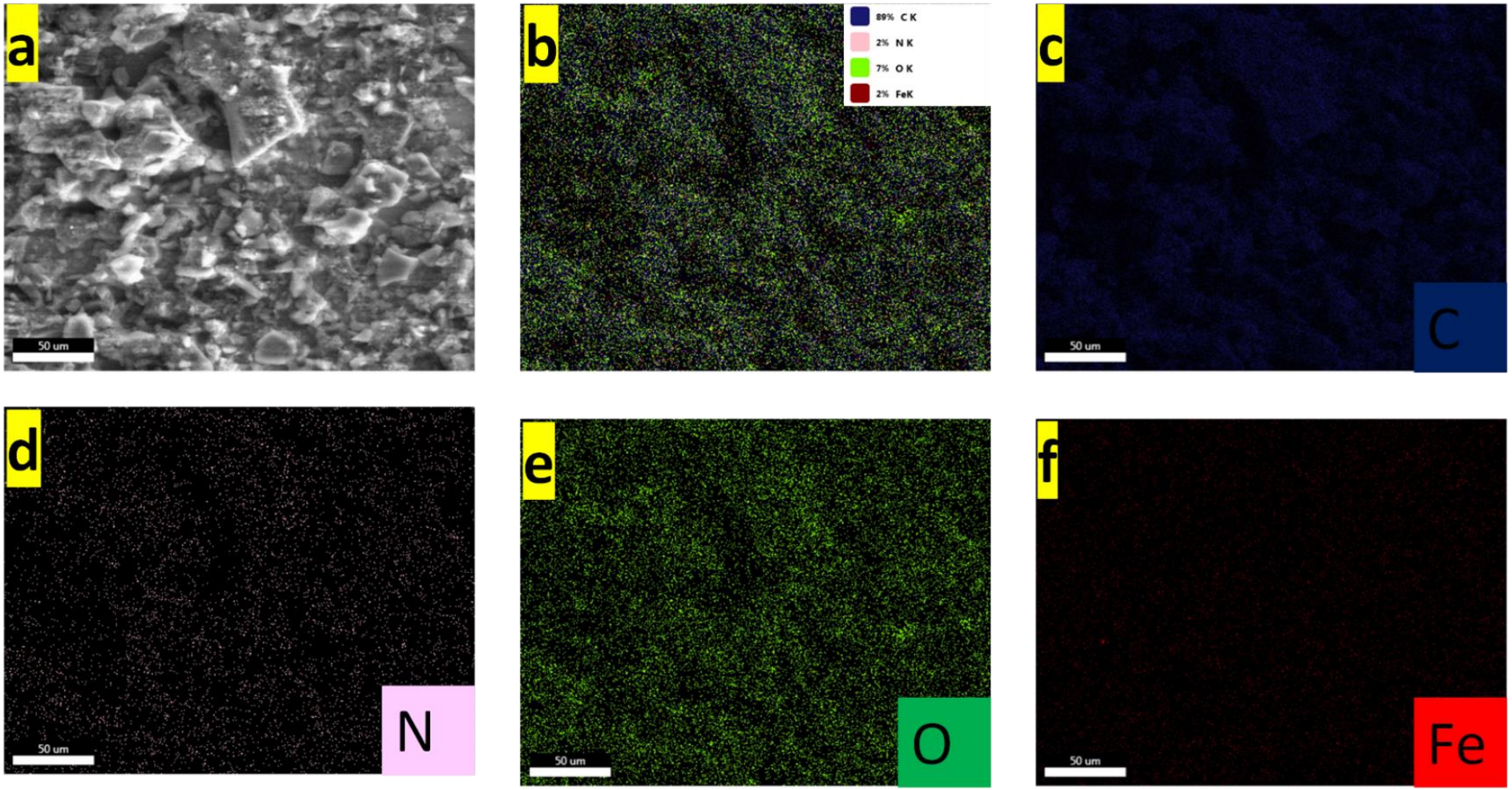

Fig. S4 Post-catalysis SEM mapping images (a-f) of FePc@SN950 on ITO coated glass plates.

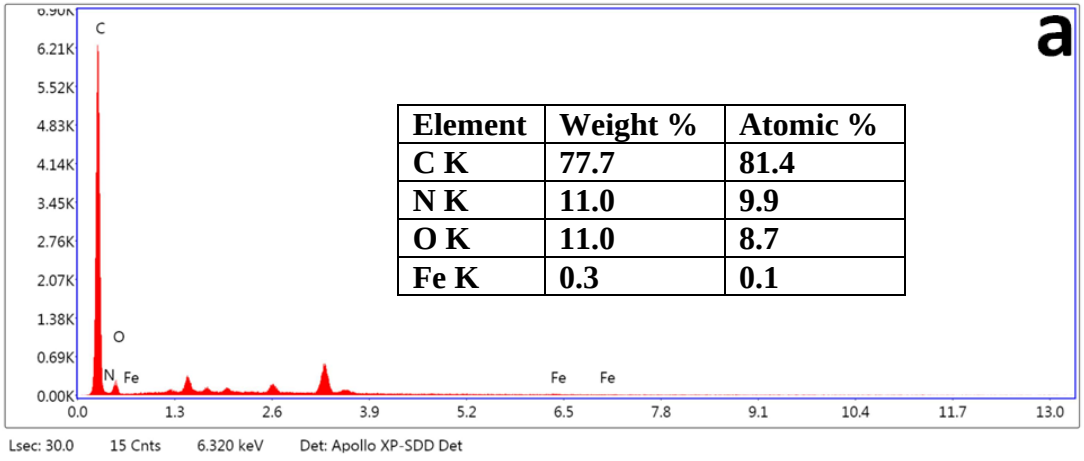

Element	Weight %	Atomic %
C K	77.7	81.4
N K	11.0	9.9
O K	11.0	8.7
Fe K	0.3	0.1

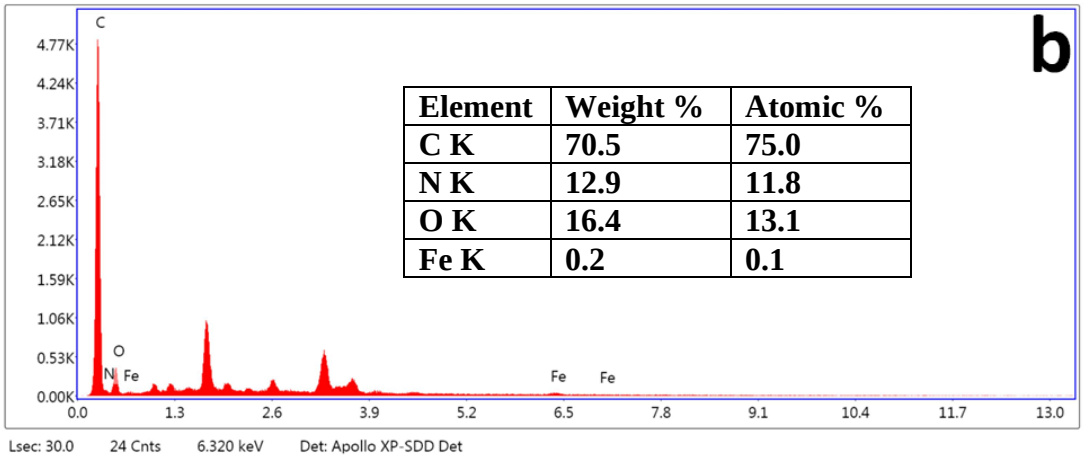

Element	Weight %	Atomic %
C K	70.5	75.0
N K	12.9	11.8
O K	16.4	13.1
Fe K	0.2	0.1

Fig. S5 EDAX spectra of pre- (a) and post- (b) catalysis FePc@SN950 on ITO coated glass plates. The inset shows the corresponding elemental composition data.

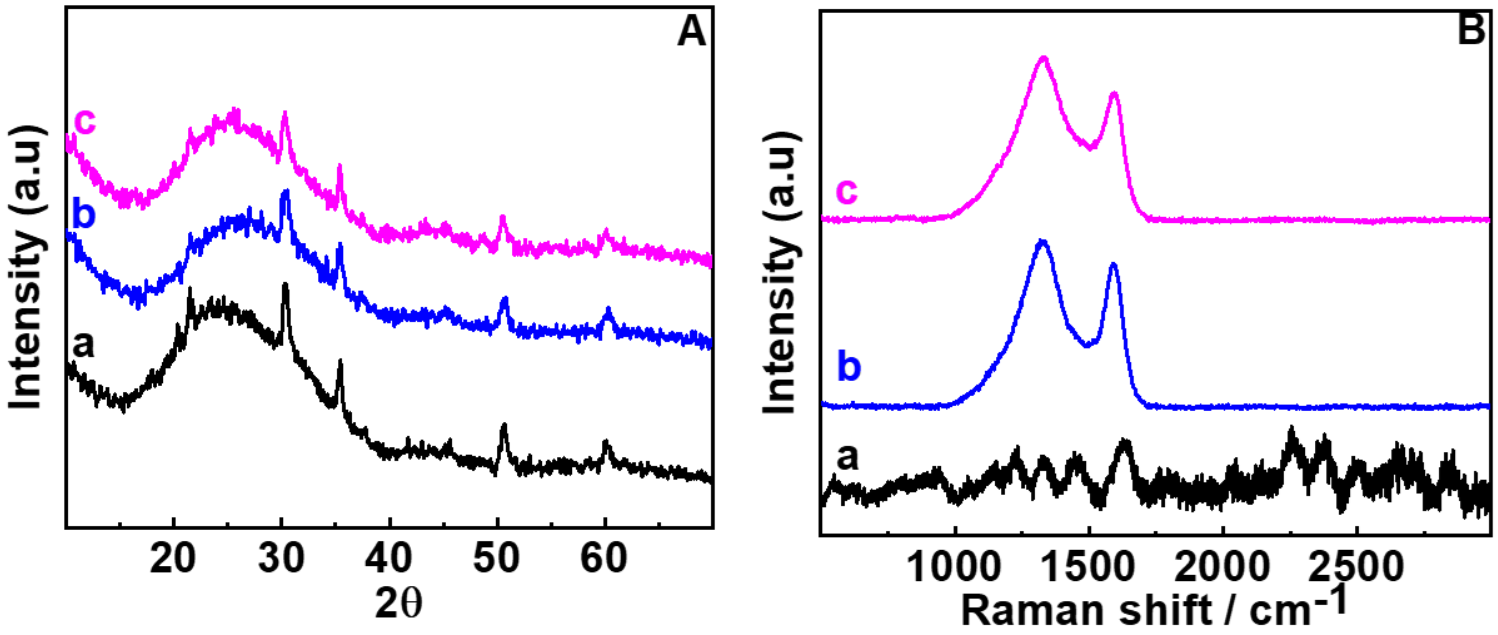

Fig. S6 Powder XRD patterns (A) and Raman spectra (B) of bare indium tin oxide coated glass plate (a) and pre- (b) and post- (c) catalysis FePc@SN950 on indium tin oxide coated glass plate.

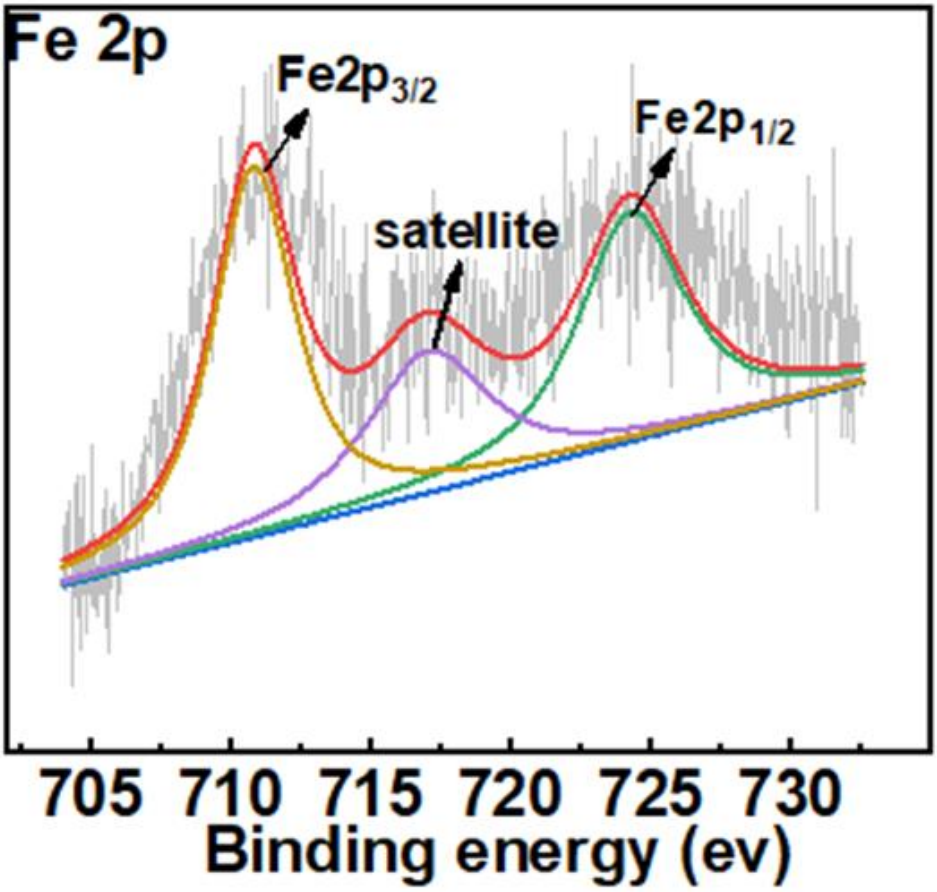

Fig. S7 Fe 2p XPS data of FePc@SN950.

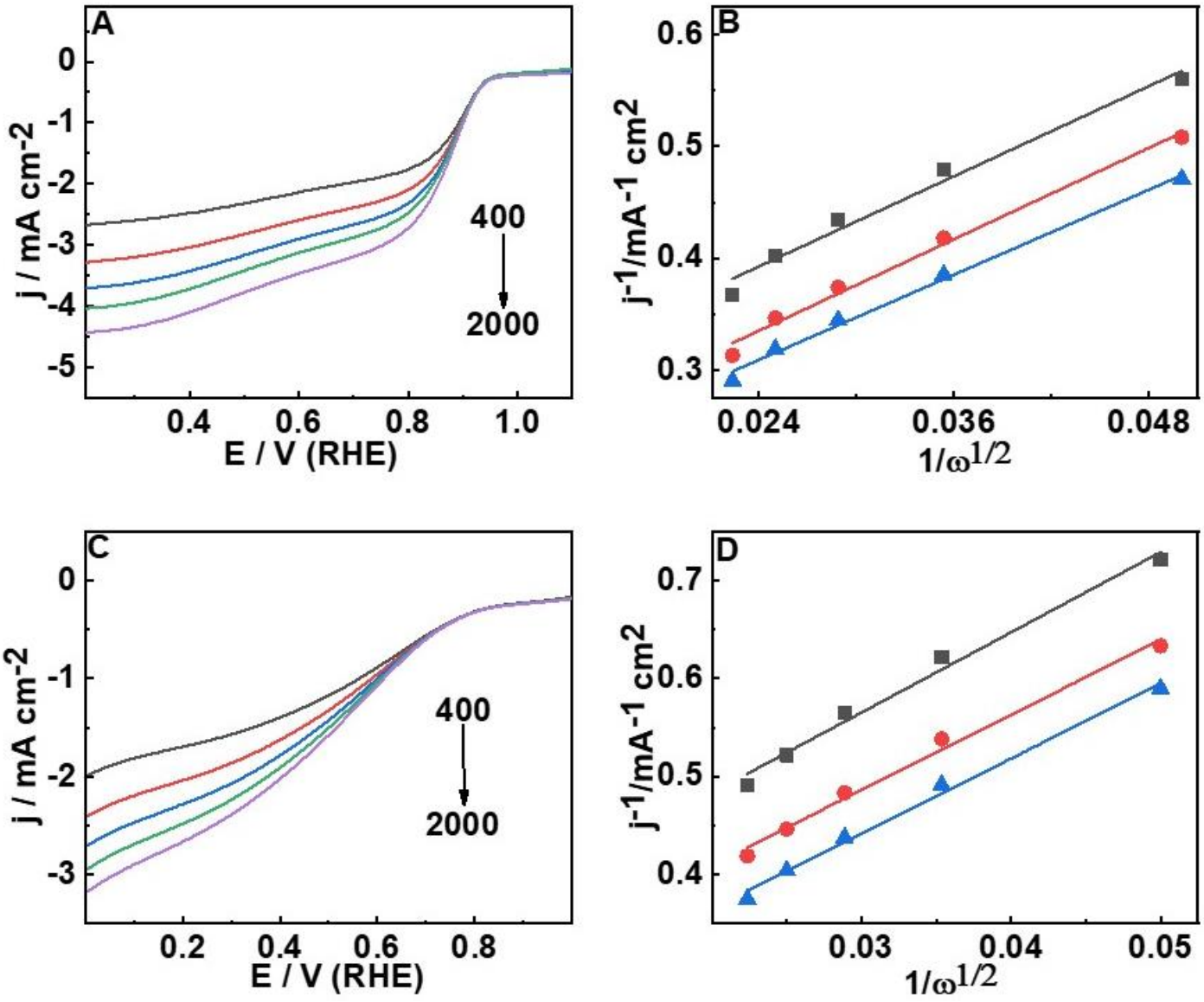

Fig. S8 LSV curves of FePc@SN950 in basic (A) and acidic (C) media and the corresponding Koutecky-Levich (K-L) plots at different potentials (B, D) and different rotation rates (400, 800, 1200, 1600, and 2000 rpm, respectively). Scan rate: 5 mVs^{-1}.

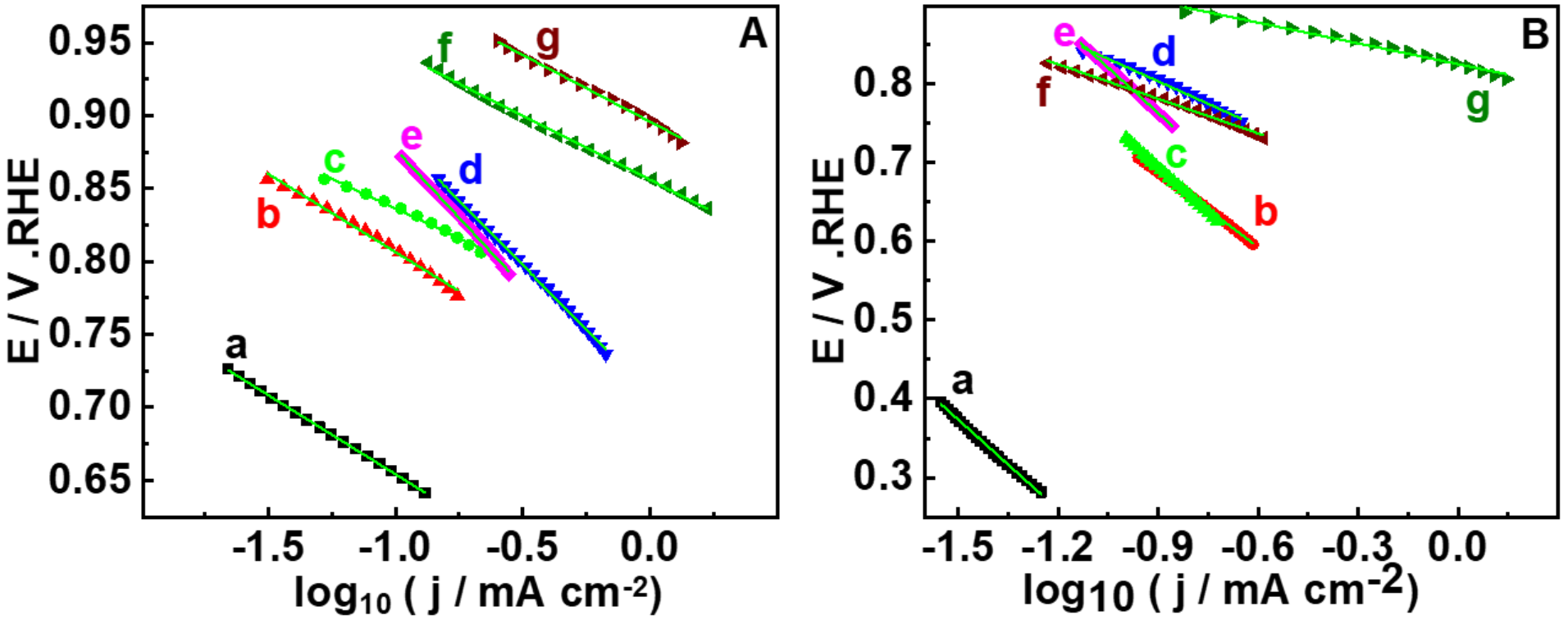

Fig. S9 Tafel slope in 0.1 M KOH (A) and 0.1 M $HClO_4$ (B) of S850 (a), S950 (b) SN850 (c), SN950 (d), SN1050 (e), FePc@SN950 (f), and Pt/C (g).

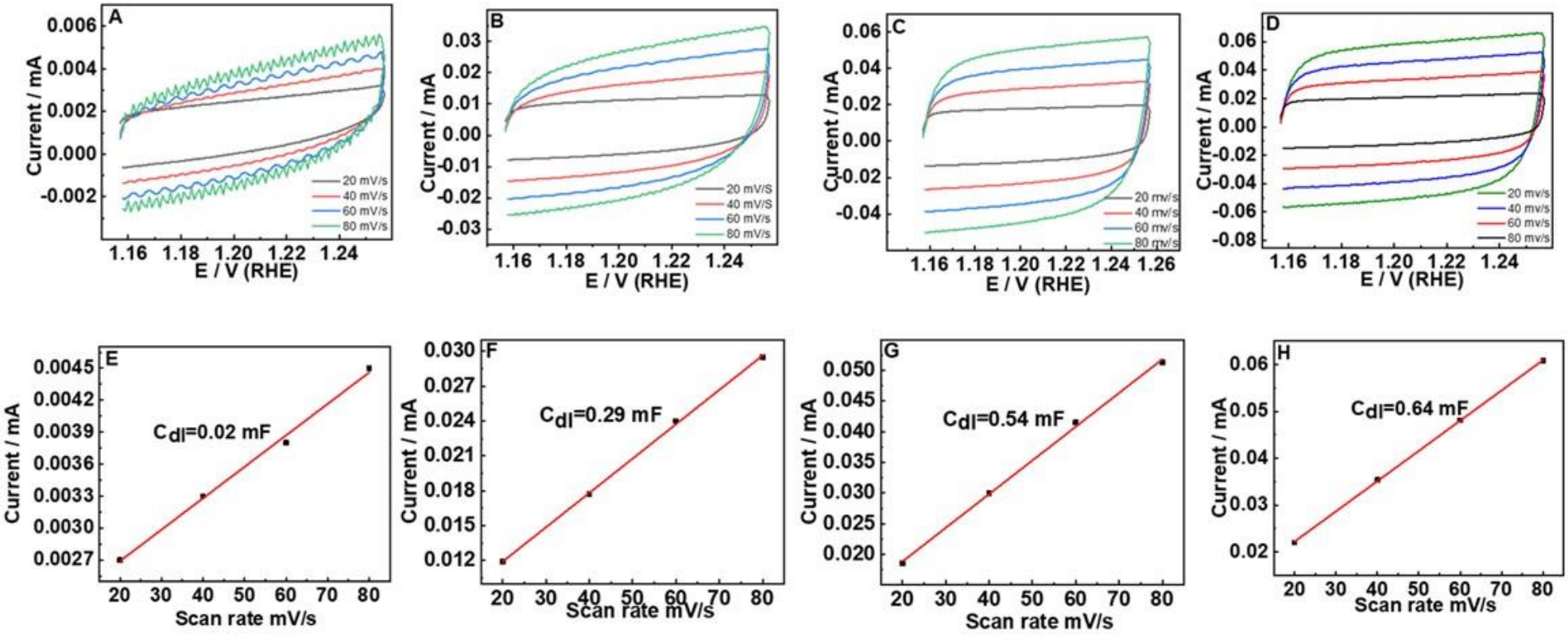

Fig. S10 CV responses (A-D) of S850 (A), SN850 (B), SN950 (C), and SN1050 (D) at different scan rates and their corresponding current density variations with scan rates (E-H, respectively).

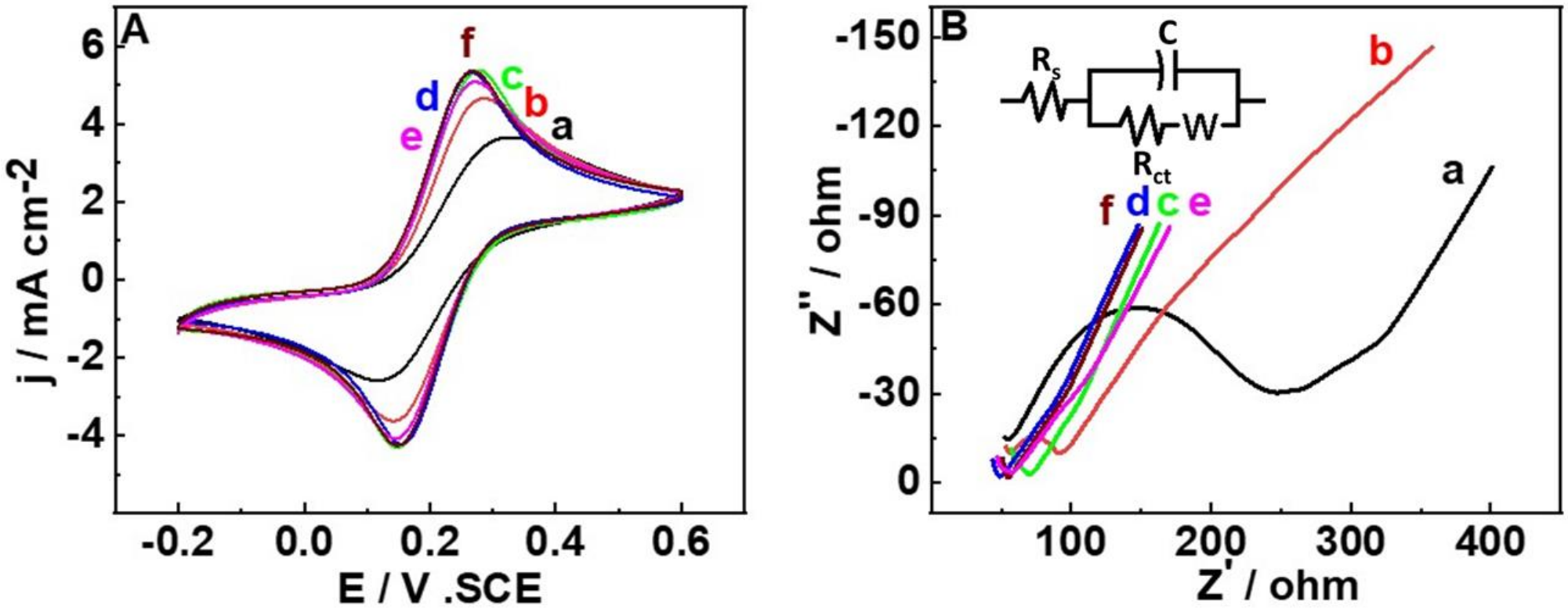

Fig. S11 CV responses at a scan rate of 20 mVs^{-1} (A) and Nyquist plots (B) of S850 (a), S950 (b) SN850 (c), SN950 (d), SN1050 (e), and FePc@SN950 (f) in 10 mM (1:1) $K_3[Fe(CN)_6]/K_4[Fe(CN)_6]$ redox probe containing 1.0 M KCl. Inset of B shows the best fit Randles equivalent circuit, where R_s is the solution resistance, C is the double layer capacitance, R_{ct} is the charge transfer resistance, and W is the Warburg impedance. Frequency: 0.1 Hz -100 KHz, Potential: 0.18 V vs $Hg/HgCl_2$

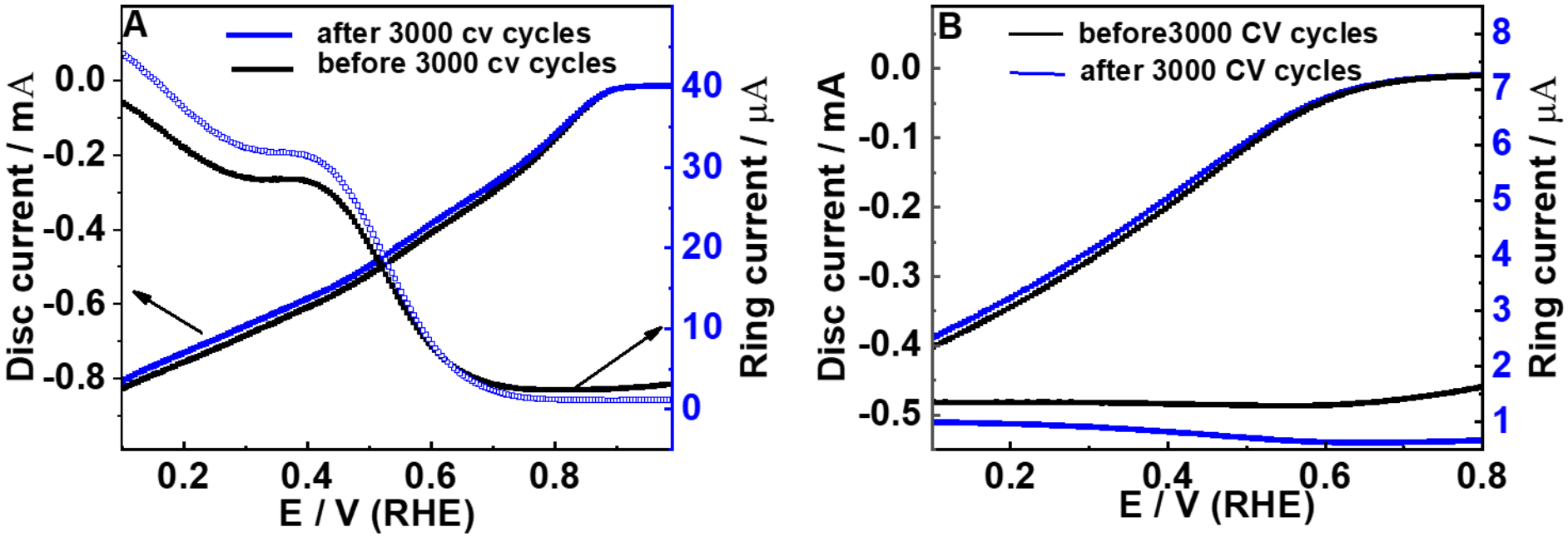

Fig. S12 Disc and ring currents in 0.1 M KOH (A) and 0.1 M $HClO_4$ (B) before and after 3000 continuous CV cycles. The disc alone was coated with FePc@SN950. The disc potential was scanned from 1.0 to 0.1 V *vs.* RHE (0.1 M KOH) and 0.8 to 0.1 V *vs.* RHE (0.1 M $HClO_4$) at a scan rate of 10 mVs^{-1} and a rotation rate of 1600 rpm. Ring potential was kept constant at 1.5 V *vs.* RHE.

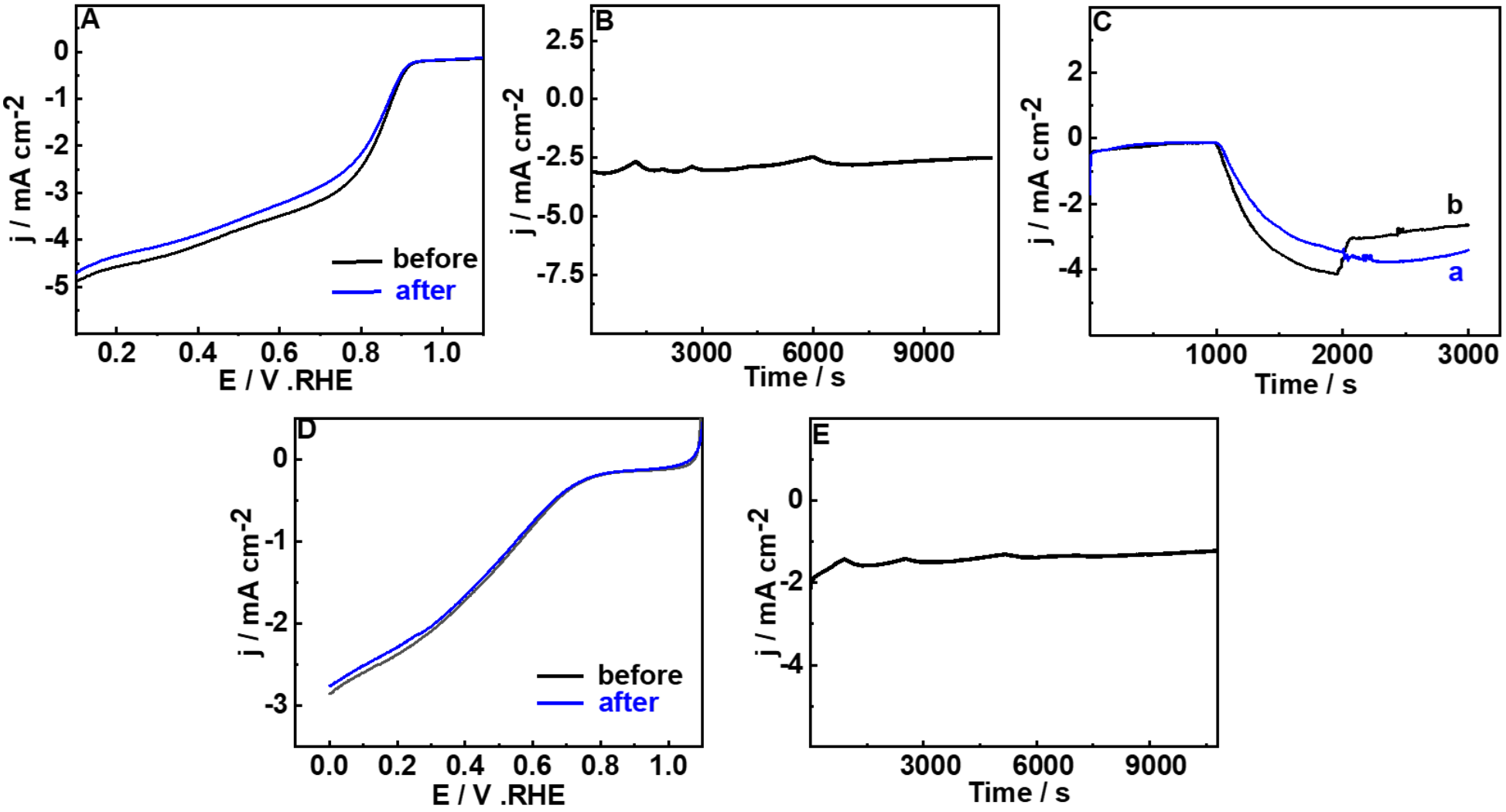

Fig. S13 LSV responses before and after 3000 CV cycles in basic (A) and acidic (D) media and amperometry stability results in basic (B) and acidic (E) media for FePc@SN950 at 0.5 V (basic) and 0.2 V (acidic) *vs.* RHE. Methanol tolerance analyzes (C) of FePc@SN950 (a) and Pt/C (b).

References

S1 B. Wang, L. Xu, G. Liu, P. Zhang, W. Zhu, J. Xia and H. Li, Biomass willow catkin-derived Co3O4/N-doped hollow hierarchical porous carbon microtubes as an effective tri-functional electrocatalyst, *J. Mater. Chem. A*, 2017, **5**, 20170–20179.

S2 P. Chen and S. Yu, N-, P- and Fe-tridoped nanoporous carbon derived from plant biomass: an excellent oxygen reduction electrocatalyst for zinc–air batteries, DOI:10.1039/c6ta02150f.

S3 W. Y. Xie, C. Ling, Z. Y. Huang, W. C. Chen, S. F. He, L. ping Si and H. Y. Liu, Metalloporphyrin doped rice husk-based biomass porous carbon materials as high performance electrocatalyst for oxygen reduction reaction in Zn-Air battery, *Int. J. Hydrogen Energy*, 2024, **51**, 857–868.

S4 K. Nernprom, J. Sanetuntikul, A. Saejio, N. Pitipuech, K. Wichianwat, N. Chanlek, C. Poompipatpong, N. Chanunpanich and K. Ketpang, Water hyacinth root derived hybrid metal oxides/nitrogen doped porous carbon as an efficient non-precious metal oxygen reduction reaction electrocatalyst in alkaline media, *Int. J. Hydrogen Energy*, 2024, **50**, 1549–1558.

S5 Y. Liu, J. Ruan, S. Sang, Z. Zhou and Q. Wu, Iron and nitrogen co-doped carbon derived from soybeans as efficient electro-catalysts for the oxygen reduction reaction, *Electrochim. Acta*, 2016, **215**, 388–397.

S6 Y. Wu, Y. Chen, H. Wang, C. Wang, A. Wang, S. Zhao, X. Li, D. Sun and J. Jiang, Efficient ORR electrocatalytic activity of peanut shell-based graphitic carbon microstructures, *J. Mater. Chem. A*, 2018, **6**, 12018–12028.